ACS OMEGA

Open Access

http://pubs.acs.org/journal/acsodf

Article

Surfactant Synergistic Effect and Interfacial Properties of Microemulsions Compounded with Anionic and Nonionic Surfactants Using Dissipative Particle Dynamics

Biao Zhang, Baoshan Guan,* Yufan Tao, Weidong Liu, Baoliang Peng, and Kai Lv

Cite This: *ACS Omega* 2024, 9, 23903−23916

Read Online

ACCESS | Metrics & More | Article Recommendations | Supporting Information

ABSTRACT: Microemulsions are one of the most promising directions in enhanced oil recovery, but conventional screening methods are time-consuming and labor-intensive and lack the means to analyze them at the microscopic level. In this paper, we used the Clint model to predict the changes in the synergistic effect of the mixed system of anionic surfactant sodium dodecyl benzenesulfonate and nonionic surfactant polyethoxylated fatty alcohols (C12E6), generated microemulsions using surfactant systems with different mole fractions, and used particle size to analyze the performance and stability of microemulsions, analyze the properties and stability of microemulsions using particle size, and analyze the interfacial behaviors and changes of microemulsions when different systems constitute microemulsions from the point of view of mesoscopic microemulsion self-assembly behaviors by combining with dissipative particle dynamics. It has been shown that microemulsion systems generated from anionic and nonanionic surfactants with a synergistic effect, based on the Clint model, exhibit excellent performance and stability at the microscopic level. The method proposed in this paper can dramatically improve the screening efficiency of microemulsions of anionic and nonanionic surfactants and accurately analyze the properties of microemulsions, so as to provide a theoretical basis for the subsequent research on microemulsions.

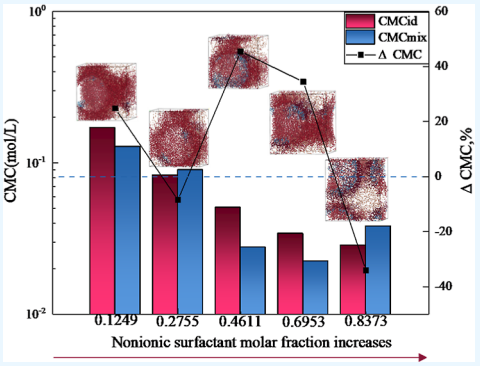

1. INTRODUCTION

Petroleum, as a crucial nonrenewable resource and strategic reserve, plays a decisive role in the economy and development.[1] However, primary oil recovery techniques that rely on the original formation energy and secondary techniques that involve water injection can only extract around 30% of the formation reserves.[2] Moreover, as exploration and development progress, unconventional geological conditions such as low permeability[3] and tight reservoir[4] become more prevalent, rendering simple extraction methods inadequate for further enhanced oil recovery (EOR).[5] In the field of EOR, chemical flooding like surfactant flooding,[6] polymer flooding,[7] and combination flooding[8] have been developed to achieve this goal. Among these methods, microemulsion has recently gained attention as a promising approach in the field of chemical flooding for its potential to enhance oil recovery.[9]

Microemulsions possess certain characteristics such as ultralow interfacial tension (IFT) and high solubilizing capacity,[10] making them widely applicable in industries such as cosmetics,[11] pharmaceuticals,[12] and petroleum.[9,13,14] In the petroleum industry, microemulsions can overcome issues, such as phase separation and instability commonly associated with conventional chemical flooding emulsions, providing better stability. A microemulsion is a solution that spontaneously forms when two immiscible liquids, typically water and hydrocarbon, are present along with a surfactant and auxiliary alcohols.[15] It is usually a transparent or semitransparent solution, generally with particle sizes in the range of 5−100 nm,[16] with thermodynamic properties.[16,17] Microemulsion solubilize both oil and water and exhibit extremely low IFT with both phases.[18] During the oil displacement process, capillary forces are almost negligible, and microemulsions possess a strong solubilizing capacity for residual oil along the course. This results in significantly improved sweep efficiency and displacement efficiency,[19] making microemulsion one of the most promising chemical flooding for EOR.

Winsor classified systems as Winsor type I, Winsor type II, and Winsor type III based on whether they coexisted with excess oil and water at equilibrium.[20] Winsor type I (upper segment) and Winsor type II (lower segment), respectively, and are classified as O/W and W/O microemulsions.[21] W/O microemulsions coexist with an excess water phase, where the surfactant forms reversed-phase micelles in the oil phase, while

Received: March 1, 2024
Revised: May 8, 2024
Accepted: May 13, 2024
Published: May 21, 2024

water is solubilized into the core of the micelles. Winsor type III is a center phase microemulsion that coexists with excess oil and water in three phases. The oil and water within the intermediate phase form a continuous phase, creating an interlocking spatial mesh structure with a highly flexible interface that is more susceptible to deformation.[22] This structure possesses high surface−interfacial activity and solubilization capacity.[23]

Several theories exist regarding the formation of microemulsions, including the instantaneous negative IFT theory[24] proposed by Schulman and Prince based on the Gibbs formula,[25] the packing parameter theory,[26] the Interface adsorption film theory,[27] and the R-ratio theory.[13] However, there is currently no guiding theory for the choice of microemulsion composition, ratio, or use of microemulsions in the field. In the oilfield, the process of selecting microemulsion formulations requires extensive testing and screening. Traditionally, parameters such as oil−water ratio, surfactant concentration, or salinity in microemulsion systems are adjusted by methods such as fish phase diagram method[28] or phase titration, and formulation performance is tested by characterization methods such as IFT test, small angle neutron scattering (SAXS),[29] microfluidic test,[30] or core displacement test in EOR.[14] Experimental methods like standing stability tests, IFT measurements, and particle size distribution analysis are employed to evaluate the performance of microemulsions and screen different formulations. For instance, Carrillo[31] et al. conducted a study on the phase behavior of microemulsions prepared with various anionic and nonionic surfactants in different molar ratios, examining their influence on phase volume. The synergistic use of nonionic and anionic surfactants makes the aggregation and interfacial behavior of micelles more complex, and researchers often use methods such as the regular solution theory of mixed micelles to construct the interaction coefficients and critical micelle concentrations between different types of surfactants from parameters such as the mole fraction of the binary mixtures and the total concentration of the surfactant binary mixtures in aqueous solution.[32] Sripriya[33] et al. investigated the phase behavior of microemulsions prepared with hydrocarbons of varying chain lengths (such as *n*-octane, *n*-decane, *n*-dodecane, etc.). These studies demonstrate that conventional screening methods for microemulsions are time-consuming and lack theoretical guidance for surfactant compounding. Consequently, performance testing remains the primary option, while a deeper understanding of molecular mechanisms is still lacking.

Molecular simulation techniques in computer science provide efficient means to overcome experimental limitations and enable more efficient simulation, observation and analysis at the molecular level.[34,35] Conventional molecular simulation methods include dynamic density functional theory at the quantum mechanical level, molecular dynamics simulation at the molecular level, and Monte Carlo simulation.[36] However, conventional molecular dynamics methods are limited in terms of the simulation size. For example, the gold standard molecular dynamics simulation is typically conducted with around 10,000 atoms (nanoscale) and analyzed for 10 ns or less.[35] The spatial and temporal dimensions of dynamic density functional theory in quantum mechanics are even smaller, involving only a few hundred atoms and picosecond timescales. As the model size and simulation time increase, the computational power required by the computer exponentially grows, making model calculations and analyses longer and more expensive than those of real experiments. This contradicts the original intention of using computer simulation techniques for an efficient and rapid analysis. Consequently, molecular dynamics models are often employed to study small-scale motions and diffusive behavior. However, models of multicomponent solutions, such as microemulsions, necessitate larger simulation scales and longer simulation times to achieve equilibrium among the components.[37] To address this, several mesoscopic or coarse-grained simulation methods have been developed.[38] One of the most effective methods at the mesoscopic level is dissipative particle dynamics (DPD). DPD was originally proposed by Hoogerbrugge and Koelman,[39] the coarse-grained dynamics of which obeys the Navier−Stokes equations and preserves hydrodynamics. DPD simplifies the molecular structure of the system, models its structural, thermodynamic, and transport properties through systematic discretization and classifies inter- and intramolecular dissipative forces.[37] It calculates the dynamic behavior of the system based on molecular dynamics. Compared to molecular dynamics simulations, DPD can take longer time steps and is more suitable for simulating solution systems with complex components, such as polymer,[40] surfactant,[41] gels,[42] and microemulsions.[39] In a study conducted by Li[43] et al., the interfacial behavior of sodium dodecylbenzenesulfonate [surfactant sodium dodecyl benzenesulfonate (SDBS)] and sodium oleate (OAS) surfactants in oil−water emulsification was investigated using DPD and the study revealed that the stacking behavior on the interfacial film is influenced by the surfactant concentration and the structure of the hydrophobic tail in the oil phase. Tight stacking occurs when the surfactant tail and oil molecule have similar structures. More and more scholars are beginning to use DPD technology to conduct microemulsion-related research.

This study evaluates and predicts the interfacial film parameters of a mixed system composed of nonionic surfactant polyethoxylated fatty alcohols (C12E6) and anionic SDBS. The evaluation is based on the synergistic effect of nonionic surfactants and anionic surfactants. The surface tension of the mixed surfactants was tested using the Clint model,[44] which describes the synergistic effect of anionic and nonionic surfactants. Experimental methods such as particle size and IFT were used to evaluate the performance differences of microemulsions composed of different surfactant blend systems. The interaction parameters between surfactants were analyzed at the molecular level by using research methods of molecular dynamics and DPD. The interfacial behaviors of surfactant systems constituting microemulsions were analyzed at the mesoscopic level. This analysis included studying the interfacial behaviors and interfacial parameters of the microemulsions. The study also examined a microemulsion system synergistically composed of a nonionic surfactant and anionic surfactant from multiple perspectives. The changes in the interfacial behaviors and properties of the microemulsion with changes in the molar fractions of the components were analyzed to predict the properties of the microemulsion generated from the anionic and nonionic surfactant system.

2. MATERIALS AND METHODS

2.1. Materials. Dodecylhexaethylene glycol (C12E6) and sodium dodecyl benzenesulfonate (SDBS) were purchased from Aladdin (China) with a purity of >99.8 wt %. Dodecane was purchased from Aladdin (China) with a purity of >99.8 wt

https://doi.org/10.1021/acsomega.4c01933
ACS Omega 2024, 9, 23903−23916

% and isopropanol was purchased from Aladdin (China) with a purity of >99.8 wt %. All deionized water with resistivity of 18.0 MΩ cm in the experiment was obtained using a purification system (UPH-I-10 T, Petroleum Exploration and Development Institute, China). Staining of alkanes and deionized water was carried out using Sudan Red III and methylene blue, respectively.

2.1.1. Surface Tension Measurement. The surface tension of all solutions was tested using Theta Lite Optical Contact Angle Measuring Instrument (Biolin, Suomi), based on the pendant drop method, surface tension was tested at 25 °C, and all surfactant solutions were formulated at 1.5 wt % NACl. Droplet shape fitting method was based on Young−Laplace method. The surface tension is then calculated by the following equation[45]

$$\sigma = \frac{\Delta\rho \mathrm{d}e^2 g}{H} \tag{1}$$

where σ is the surface tension of the solution, mN/m; $\Delta\rho$ is the density difference between the solution and air, g/cm^3; de is the maximum diameter of the droplet when it approximates to a spherical shape, ds is the minimum diameter of the droplet, and H is obtained from the Misak model,[46] H = de/ds. The parameters for surface tension calculation are detailed in the Supporting Information.

2.1.2. Laser Particle Sizing. MAS OPTION automatic particle sizer (USA) was used to measure the particle size of microemulsions. Designed for use with either concentrated suspensions of small particles or solutions of macromolecules. The tested particle sizes range from 2 nm to 3 μm. The measurement method is as follows: particle sizer is turned on and warmed up for 30 min, the liquid to be measured is injected into the cuvette to 70−80%, and warmed up for 3 min at 25 °C; then, it will be placed in the cuvette of the particle sizer to use the particle size measurement, the running duration of two min each time, and then take the average of three times of testing to get the microemulsion particle size distribution.

2.2. Simulation Method and Detail. *2.2.1. DPD Methods and Simulation Detail.* DPD can simulate complex fluid motions for large spaces and long timescales on a mesoscopic scale.[37] In the DPD simulation, the molecular structures of the complex were coarse-grained into discrete beads, ignoring the details of the molecular structure and degree of freedom. Each bead is a carrier with mass attributes, reflecting the motion change of the fluid.

In a DPD system, coarse-grained beads follow the Newtonian eq 2 of motion

$$\frac{\mathrm{d}\vec{r}_i}{\mathrm{d}t} = v_i, \qquad m_i \frac{\mathrm{d}\vec{v}_i}{\mathrm{d}t} = \vec{f}_i \tag{2}$$

where $\vec{r}_i$ and $\vec{f}_i$ represent the vector, velocity, and total force at the position of the i position bead, respectively.

The superposition of the three forces and their subsequent motions are the force equation on the mesoscopic level for the coarse-grained model. There are mutual forces between the coarse-grained beads, as shown in eq 3

$$\vec{F} = \sum_{i \neq j} (\vec{F}_{ij}^{D} + \vec{F}_{ij}^{C} + \vec{F}_{ij}^{R}) \tag{3}$$

where $\vec{F}_{ij}^{D}$ refers to the dissipative force, which describes the friction dissipation between the structural system in the simulated bead. $\vec{F}_{ij}^{C}$ is the conservative force that describes the repulsive properties between coarse grained beads. $\vec{F}_{ij}^{R}$ is the random force that simulates Brownian random motion at ambient temperatures.

The dispersive and random forces act as a heat sink and source, respectively, consequently, their combined effect is a thermostat.[47] The conservative forces are in the form of

$$\vec{F}_{ij}^{C} = \begin{cases} a_{ij}\left(1 - \frac{r}{R_c}\right); & r \leq R_c \\ 0; & r > R_c \end{cases} \tag{4}$$

$$\vec{F}_{ij}^{D} = -\gamma_{ij}\omega_D(r)(\hat{r}\cdot v)\hat{r} \tag{5}$$

where a_{ij} is the distance between the beads i and j. R_c is the interaction radius of the dimensions of the simulation system. The parameter a_{ij} is the hydrodynamic interaction parameter that contains the physical−chemical information relevant to the atomic group.

We can use the Flory−Huggins model to calculate the a_{ij} parameter in DPD.

$$k^{-1} = 1 + 2\alpha a_{ii}\overline{\rho} \tag{6}$$

where k^{-1} is the dimensionless isothermal compressibility; a_{ii} is the self-repulsive conservative parameter; α is the correction coefficient; $\overline{\rho}$ is the density of the system. Groot and Warren established a link between a_{ij} and Flory−Huggins parameter χ_{ij}.

$$a_{ij} = 25 + 3.5\chi_{ij} \tag{7}$$

In this emulsification simulation system, χ_{ij} is the Flory−Huggins parameter,[48] so the obtained χ_{ij} can establish that the force field is under DPD.

$$\chi_{ij} = \frac{v_b}{k_b T}(\delta_i - \delta_j)^2 \tag{8}$$

where, v_b is the average molar volume of beads i and j, Å^3; δ_i and δ_j are the solubility parameters of the coarse-grained beads i and j, respectively. k_bT is the environmental value of the system.

The volume of coarsely granulated beads is calculated as shown in eq 9[49]

$$V_{CG} = \frac{M_{CG}}{N_A} \tag{9}$$

where V_{CG} is the volume of the coarsely granulated beads, Å; M_{CG} is the relative molecular mass of the coarsely granulated beads, cm^3/mol; and N_A is Avogadro's constant.

Solubility parameters were calculated using Materials Studios software (USA) under the COMPASS force field: cells were modeled using Amorphous Cell, with the basic structure of coarse beads of 100 units incorporated into each cell; the models were structurally optimized as follows: (1) 100 ps *NVT*-MD simulations at 298.15 K; (2) 100 ps *NVT*-MD simulations at 298.15 K; (3) 100 ps *NPT*-MD simulations at 1 bar and 298.15 K; and (4) task calculations to obtain the coarse-grained structure of the solubility parameter, utilizing the cohesive energy density.

https://doi.org/10.1021/acsomega.4c01933
ACS Omega 2024, 9, 23903−23916

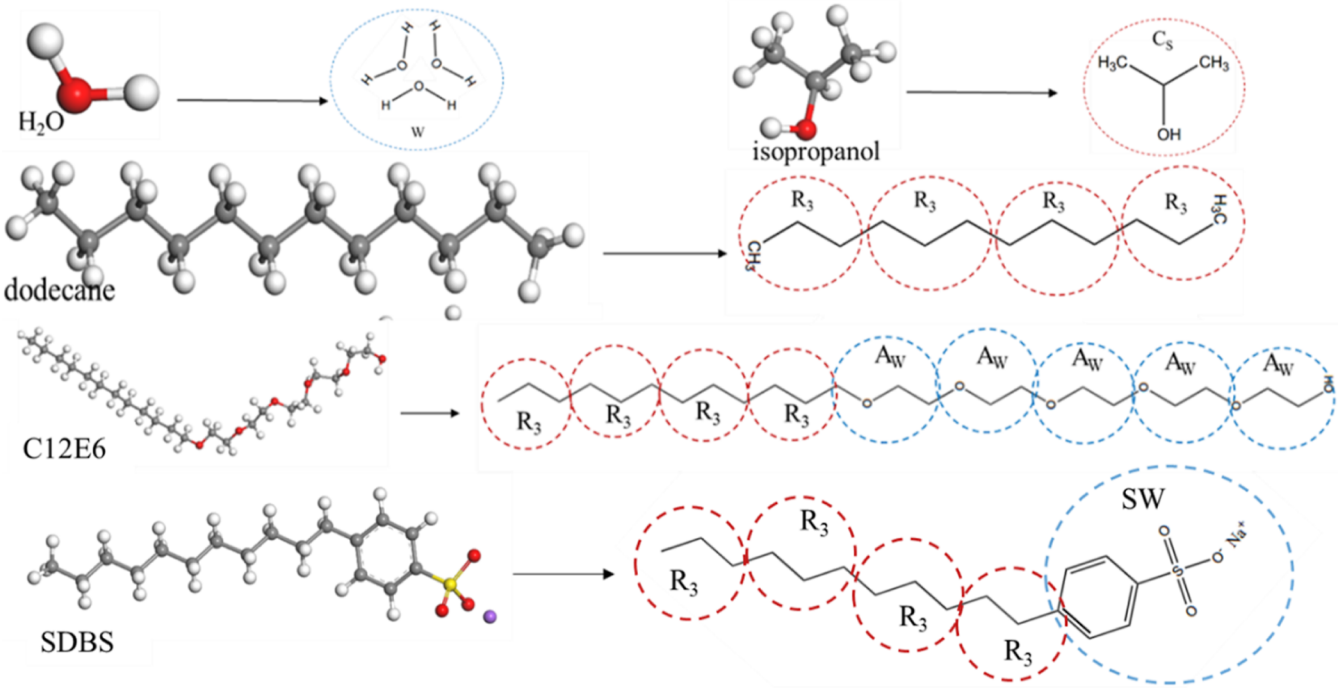

Figure 1. Plot of microemulsion components and different coarse-grained bead divisions.

2.2.2. Coarse-Grained Beads and Model Details. Reference to the methodology of Ruiz-Morales,[50] the molecular model of all components in the DPD model and the division of coarse-grained beads are shown in Figure 1, and the volume and solubility parameters of all beads can be found in Table 1.

Table 1. DPD Simulation of Volume and Solubility Parameters of Coarsely Granulated Beads

beads	molar volume of beads, Å^3	solubility parameter (cal/cm^3)$^{1/2}$
AW	74.713	29.790
AO	46.5	16.797
R3	69.7	17.597
SW	298.8	44.486
CS	99.6	23.061
W	30.0	49.867

The dimensions of the DPD model of the microemulsion are (150 × 150 × 150) r_c^3 (15 nm^3). The simulated ambient temperature is T = 298.15 K; the density of the system is ρ = 3. The number of beads in the simulated system is 2.1 × 10^5, and each DPD model is computed for 10 ns. The energy versus temperature curves of the system can be found in Supporting Information. The use of periodic boundaries[51] for the model is to eliminate the effect of boundaries on the results. A table of DPD repulsive force parameters can be found in the Supporting Information.

3. RESULTS AND DISCUSSION

3.1. Critical Micelle Concentrations of Surfactant Systems. Figure 2 illustrates a decreasing trend in the surface tension of the surfactants as the surfactant concentration increases. It can be observed that both C12E6 and SDBS exhibit a sudden decrease in surface tension followed by a leveling off as the concentration increases. This behavior occurs when the number of surfactant molecules surpasses the

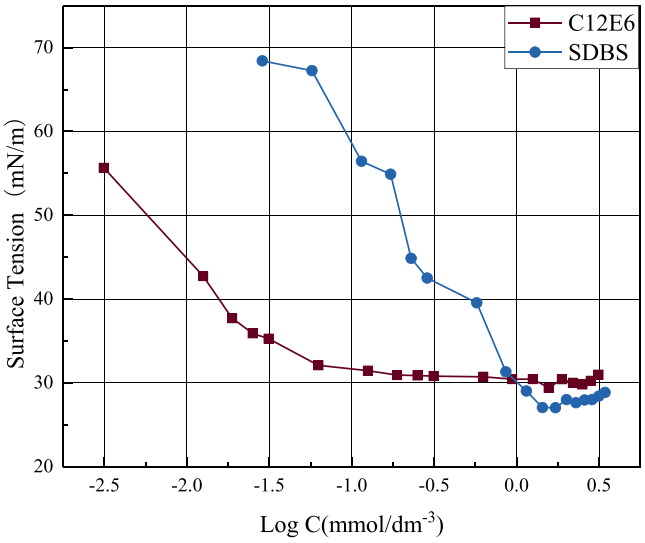

Figure 2. Surface tension of nonionic surfactant C12E6 and anionic surfactant SDBS with molar concentration.

CMC, causing them to aggregate from individual ions or molecules into micelles. To determine the CMC of the surfactant system, a segmented linear fit was performed before and after the inflection point of the surface tension−concentration curve. The intersection of the two fitted straight lines was the CMC. The CMC of pure C12E6 was determined to be 0.0238 mmol/dm^{-3}, while that of pure SDBS was 1.3668 mmol/dm^{-3}, which aligns generally with previously reported surface tension values in the literature.[52] The CMC of C12E6 was significantly lower than that of SDBS. This difference can be attributed to the fact that the CMC of nonionic surfactants is mainly influenced by the length of their hydrophilic groups [i.e., the number of poly(ethoxylate) units, n] and hydrophobic groups. As the number of poly(ethoxylate) units increases, the CMC decreases rapidly. Consequently, the longer hydrophilic

https://doi.org/10.1021/acsomega.4c01933
ACS Omega 2024, 9, 23903−23916

chain length of C12E6 results in a much lower CMC compared to SDBS.

The nonionic surfactant C12E6 has a relatively low CMC, a property that facilitates microemulsion generation because it allows microemulsions to break through the critical microemulsion concentration or ($c\mu c$) at lower concentrations, thus promoting microemulsion generation. In comparison, anionic surfactant SDBS has a higher CMC than nonionic surfactants. However, anionic surfactants possess a stronger ability to reduce IFT compared to nonionic surfactants.[53] This is because anionic surfactants exhibit electrostatic repulsion between their molecules, facilitating their adsorption at the interface. On the other hand, nonionic surfactants lack electrostatic interactions and rely solely on van der Waals forces and hydrophobic interactions, resulting in a weaker adsorption ability at the interface. Therefore, the combination of anionic surfactants with nonionic surfactants enables microemulsions to surpass the CMC at lower surfactant concentrations while maintaining higher interfacial activity for solubilizing the microemulsion.

3.1.1. Surfactant Interfaces Synergetic Effect Analysis. Figure 3 presents the results of surface tension testing for

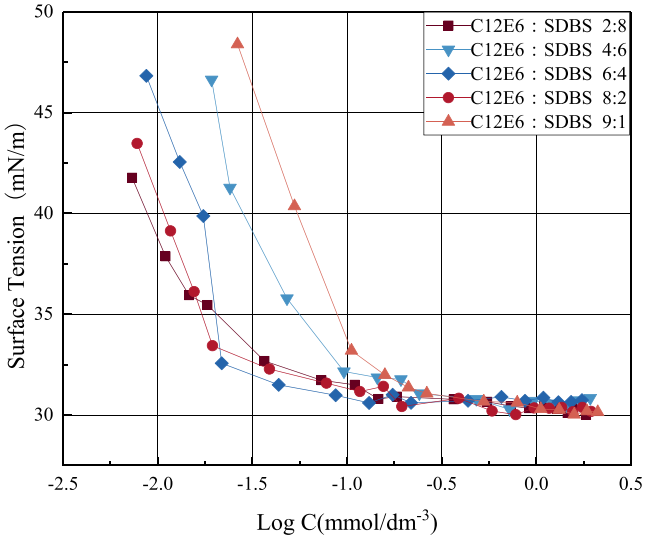

Figure 3. Plot of surface tension as a function of logarithm of molar concentration for surfactant systems with different mass ratios.

anionic and nonionic surfactant systems with varying molar fractions. It is evident that the CMC decreases significantly when the anionic surfactant is combined with the nonionic surfactant. This decrease can be attributed to the formation of mixed micelles between the anionic and nonionic surfactants, which reduces the difficulty of micelle formation and facilitates the generation of microemulsions at lower concentrations. The surface tension data for the five proportions of the surfactant system shown in the figure were fitted using segmented linear fitting. This analysis allows us to determine the CMC of the surfactant systems under the five different molar fractions, as summarized in Table 2.

Based on the Clint model,[44,54] the ideal CMC (CMC_{id}) was calculated for surfactants mixed in different molar ratios (y_1 for C12E6 molar fraction and y_2 for SDBS molar fraction). The Clint model provides a theoretical framework for micellization in surfactant systems, assuming ideal mixing within the micelles and a simple phase separation model.[55] This allows the calculation of the concentration of each monomer species and the micelle composition as a function of the total concentration, as shown in eq 10. Table 2 presents the values of the ideal CMC for an anionic nonsurfactant solution in the ideal case, obtained from the Clint model. By comparing the CMC_{id} with the CMC_{mix} measured through real surface tension experiments, we can determine the presence of interactions between the surfactants. When $CMC_{id} > CMC_{mix}$, it indicates an antagonistic effect between C12E6 and SDBS, suggesting that the surfactants do not exhibit improved interaction effect at this molar ratio. Conversely, when $CMC_{id} < CMC_{mix}$, it suggests a synergistic effect between C12E6 and SDBS, indicating that the surfactant mixture at this molar ratio promotes favorable interactions between C12E6 and SDBS. The analysis of CMC_{id} and CMC_{mix} for the solution at each ratio was recorded as ΔCMC in Table 1, calculated as $\Delta CMC = (CMC_{id} - CMC_{mix})/CMC_{id}$.

$$\frac{1}{CMC_{id}} = \frac{y_1}{CMC_1} + \frac{y_2}{CMC_2} \tag{10}$$

Figure 4 shows the variation of anionic and nonionic surfactants with molar fraction, the surface tension of the

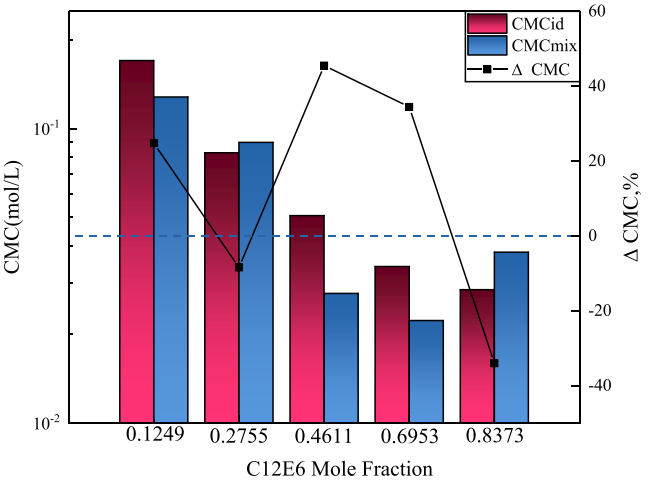

Figure 4. Plot of CMC_{id} (calculated from the Clint model), CMC_{mix} (surface tension test for the mixed system), and $\Delta CMC[(CMC_{id} - CMC_{mix})/CMC_{id}]$.

Table 2. Nonionic and Anionic Surfactant Parameters and CMC

mass ratio (C12E6:SDBS)	mole fraction of surfactant (C12E6)	mole fraction of surfactant (SDBS)	CMC_{mix} mmol/dm^{-3}	Clint CMC_{id}, mmol/dm^{-3}	ΔCMC, %
2:8	0.1249	0.8751	0.1279	0.1700	24.75
4:6	0.2755	0.7245	0.0897	0.0827	−8.42
6:4	0.4611	0.5389	0.0275	0.0506	45.51
8:2	0.6953	0.3047	0.0222	0.0340	34.48
9:1	0.8373	0.1627	0.0380	0.0283	−34.01

https://doi.org/10.1021/acsomega.4c01933
ACS Omega 2024, 9, 23903−23916

system tested CMC (CMC_{mix}) and the CMC obtained through the Clint model (CMC_{id}). For instance, when the molar fraction of the nonionic surfactant C12E6 is 0.1249 (with an anionic surfactant SDBS molar fraction of 0.8751), the system shows a synergistic effect with $CMC_{id} > CMC_{mix}$. This indicates that the two surfactants can form micelles at lower concentrations. The analysis of the decrease in CMC (ΔCMC) reveals a decrease of 24.75% when a low molar ratio of C12E6 is added. This significant decrease in the CMC is favorable for the generation of microemulsions. However, due to its low molar ratio of C12E6, the system's own CMC value is relatively high compared to other systems, which may affect the performance of microemulsions.

The CMC was analyzed under 5 M fractions. It was observed that with an increase in the SDBS molar fraction ratio, when the nonionic surfactant molar fraction is 0.2755 (with an anionic surfactant molar fraction of 0.7245), CMC_{id} is slightly smaller than CMC_{mix}. At this point, the two surfactants require a higher concentration to reach the CMC breakthrough, and the critical micelle concentrations of the nonionic and anionic surfactants are slightly lower than those of CMC_{mix}. This indicates an antagonistic effect between the nonionic surfactant and anionic surfactant. Anionic and nonionic surfactant systems were analyzed at 5 M fractions. It was found that at nonionic surfactant molar fractions of 0.4611 and 0.6953 (with anionic surfactant molar fractions of 0.5389 and 0.3047), the ΔCMC values were 45.51 and 34.48%, respectively, indicating an excellent synergistic effect. When the molar fraction of the nonionic surfactant was 0.8373 (with anionic surfactant molar fraction of 0.1627), the ΔCMC decreased to −34.01%, indicating a strong antagonistic effect between the two surfactants. The antagonism and synergy of surfactants can be further analyzed in terms of interaction parameters using molecular dynamics.

3.2. Laser Particle Size Testing of Microemulsion Systems with Different Surfactants. Microemulsions were constructed using different molar fractions of nonionic and anionic surfactant systems, dodecane acted as the oil phase in the microemulsions, isopropyl alcohol acted as a cosurfactant for the microemulsions, and electrolyte NaCl (weight concentration 1.5, 2.0%) was added in the microemulsions to promote the formation of the microemulsions, and the specific method of formulation of the microemulsions was described in the content of Supporting Information. The composition ratio of the microemulsion is shown in Table 3. For the generated microemulsions, the intermediate stable microemulsion phase was removed by using a test tube for particle size testing.

Table 3. Microemulsion Formulations

components	H_2O	dodecane	nonionic and anionic surfactants	isopropanol
mass concentration, %	42.5	42.5	6	9

As shown in Figure 5, the variation in the color of the aqueous phase caused by the variation in the concentration of the dye methylene blue does not affect the generation and properties of the microemulsion, and similarly, the color of the microemulsion in the mesophase varies with the volume of the sultan-red-stained oil phase and the methylene-blue-stained aqueous phase. Nonionic and ionic surfactants can significantly improve the interfacial activity at the interface of oil and water by reducing the electrical repulsion between charged head groups and increasing the interfacial density of adsorbed molecules, exhibiting synergistic effects, and the synergistic effects between anionic and nonionic surfactants directly affect the properties of the generated microemulsions,[56] which is most intuitively manifested in the volume of the microemulsion's midphase: with the best synergistic properties, the ratio of the microemulsion possessing the largest. The best synergistic performance was found in the midphase volume of the microemulsions: the microemulsions with the best synergistic performance had the largest midphase volume, while the microemulsions with the smallest midphase volume were found in the ratio of antagonism (0.8373:0.1627), and the overall trend was in line with the prediction of the Clint model.[55]

For the microemulsion system formed, the microemulsion particle size profile was determined by using a laser particle sizer. The results are shown in Figure 6.

The analysis of the microemulsion system generated under 1.5% NaCl revealed a peak aggregation of 34 nm at a molar fraction of C12E6 of 0.4611, indicating that this microemulsion has the smallest particle size at a molar fraction ratio of C12E6 to SDBS of 0.4611:0.5389. These findings support the stability of the microemulsion, as predicted by the Clint model. Additionally, the peak particle size of the microemulsion was measured at 53 nm for a C12E6 molar fraction of 0.6953 and 73 nm for a molar fraction of 0.1249. The microemulsion system operates as a synergistic surfactant system, generating stable and smaller microemulsions. The small particle size of these microemulsions enhances the microemulsion stability. However, when the molar fraction of C12E6 was 0.8373, the peak particle size increased to 142 nm, which was the largest of all of the systems. The thermodynamic definition of microemulsion particle size is in the range of 5−100 nm,[57] and an excessively large microemulsion particle size implies thermodynamic instability, which negatively affects the stability of microemulsions and makes them unsuitable for EOR. Furthermore, at a molar fraction of C12E6 of 0.2755, the peak particle size of the microemulsion reached 78 nm. Notably, the particle size of the microemulsion generated by the antagonistic surfactant system was significantly larger than that generated by the synergistic system. The synergistic effect between the nonionic and anionic surfactants can influence the performance of the microemulsion.

The addition of an inorganic salt significantly reduces the electrostatic repulsion between the surfactant ionic heads, facilitating micelle formation. This increase in the salt concentration promotes the performance of the microemulsion. When the NaCl concentration reached 2.0%, the overall particle size of the microemulsion decreased. The two systems with a better synergistic effect (C12E6Mole fraction 0.4611 and 0.6953) exhibited a decrease in microemulsion particle size with increasing salt concentration. Notably, at a molar fraction of 0.4611 for C12E6, the particle size of the microemulsion decreased to 22 nm. In contrast, the microemulsion system generated by the antagonistic surfactant system showed minimal decrease in particle size with increasing salt concentration, with only a small amount of microemulsion observed. The particle size test results demonstrate that the stability of the microemulsion is influenced by the synergistic effect, and the significant

https://doi.org/10.1021/acsomega.4c01933
ACS Omega 2024, 9, 23903−23916

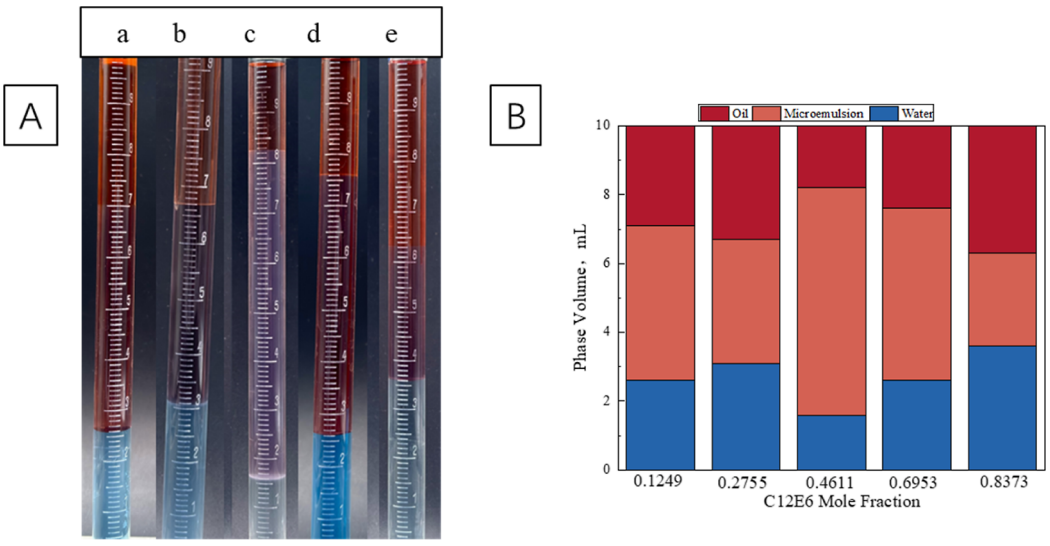

Figure 5. Schematic diagram of microemulsion formation with different molar ratios of C12E6 to SDBS. (A) Snapshots of microemulsions varying with C12E6 molar ratio: (a) C12E6 0.1249 and SDBS 0.8751; (b) C12E6 0.2755 and SDBS 0.7245; (c) C12E6 0.4611 and SDBS 0.5389; (d) C12E6 0.6953 and SDBS 0.3047; (e) C12E6 0.8373 and SDBS 0.1627; and (B) Volume stacking diagram for each of the generated microemulsions.

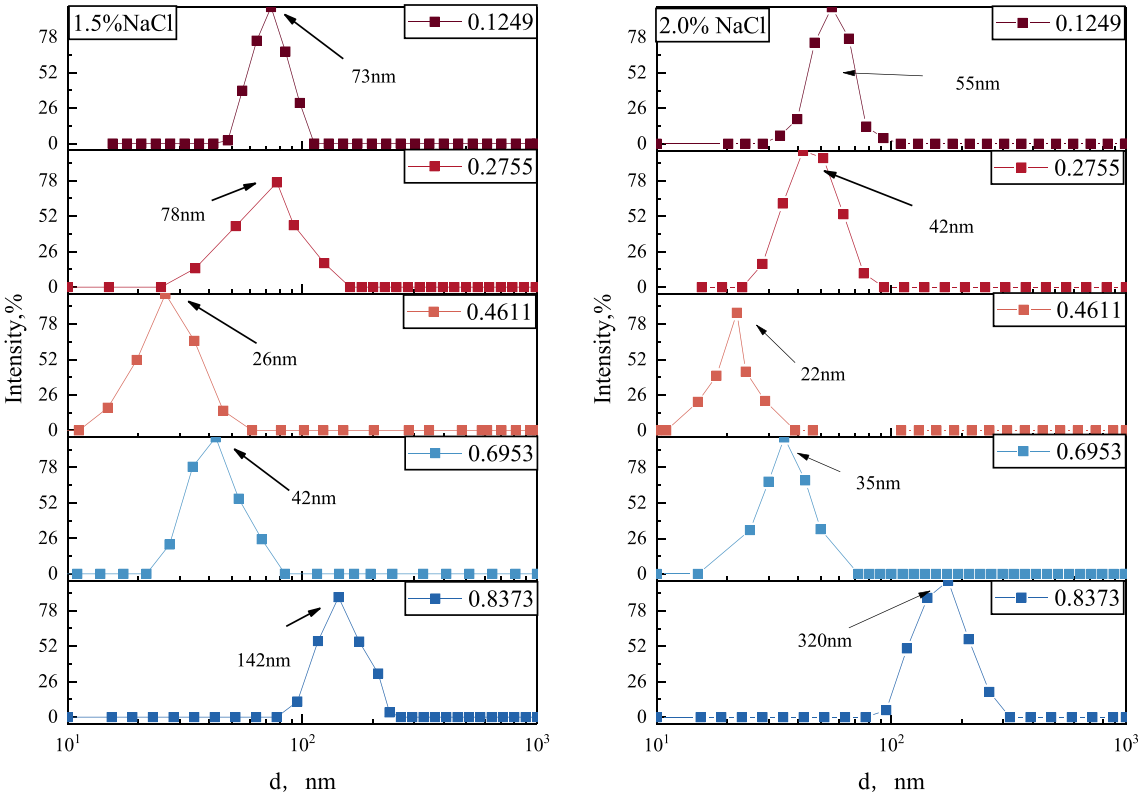

Figure 6. Microemulsions with different molar fractions of surfactant components.

difference in particle size of the microemulsion indicates unstable interfacial behavior.

3.3. Dissipative Particle Dynamics Modeling of Microemulsions with Different Molar Fraction Surfactant. A DPD model was employed to construct a microemulsion model using the anionic and nonionic surfactant systems previously described. The model included water, dodecane as the oil phase, and isopropanol as the cosurfactant, with the same molar ratios as those used in the particle size test. The particle composition of the microemulsion is depicted in Figure 7. With the dodecane content in the oil phase reaching 50%, water-in-oil microemulsions were formed in all systems. Observing Figure 2a−e, it is evident that the combination of the nonionic surfactant C12E6 and the anionic surfactant SDBS resulted in phase separation between water and dodecane. The two surfactants exhibited regular and aggregate distributions between the oil and water phases, forming the interfacial membrane of the microemulsion. On

https://doi.org/10.1021/acsomega.4c01933
ACS Omega 2024, 9, 23903−23916

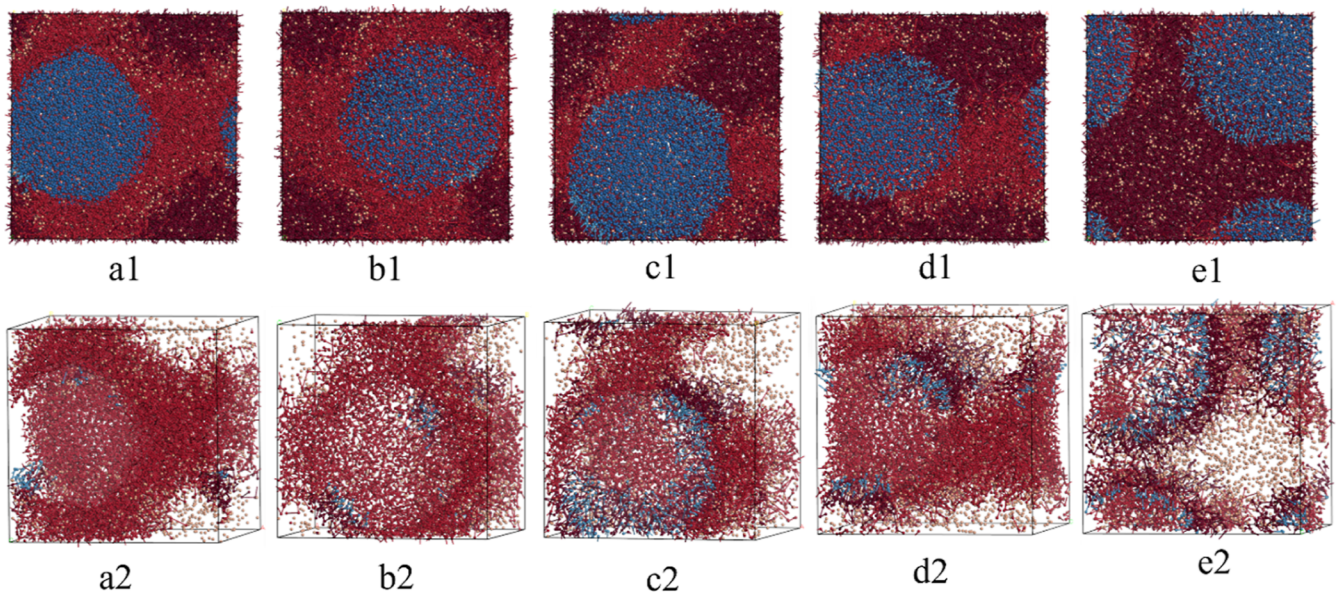

Figure 7. Snapshots (10 ns) of DPD of microemulsions formed by a surfactant system consisting of C12E6 and SDBS with dodecane, water, and isopropanol. The dark red beads in the model are dodecane, red beads are C12E6, pink beads are isopropanol, blue beads are SDBS, and dark blue beads are H_2O. In all models, the concentration of dodecane was 50%, the concentration of water molecules was 23%, the concentration of cosurfactant isopropanol was 7%, and the total concentration of C12E6 with SDBS was 20%. (a1−e1) Are 10 ns snapshots of all components and (a2−e2) are 10 ns snapshots of interface film. Surfactant mole fraction: (a1,a2) C12E6 0.1249 and SDBS 0.8751; (b1,b2) C12E6 0.2755 and SDBS 0.7245; (c1,c2) C12E6 0.4611 and SDBS 0.5389; (d1,d2) C12E6 0.6953 and SDBS 0.3047; and (e1,e2) C12E6 0.8373 and SDBS 0.1627.

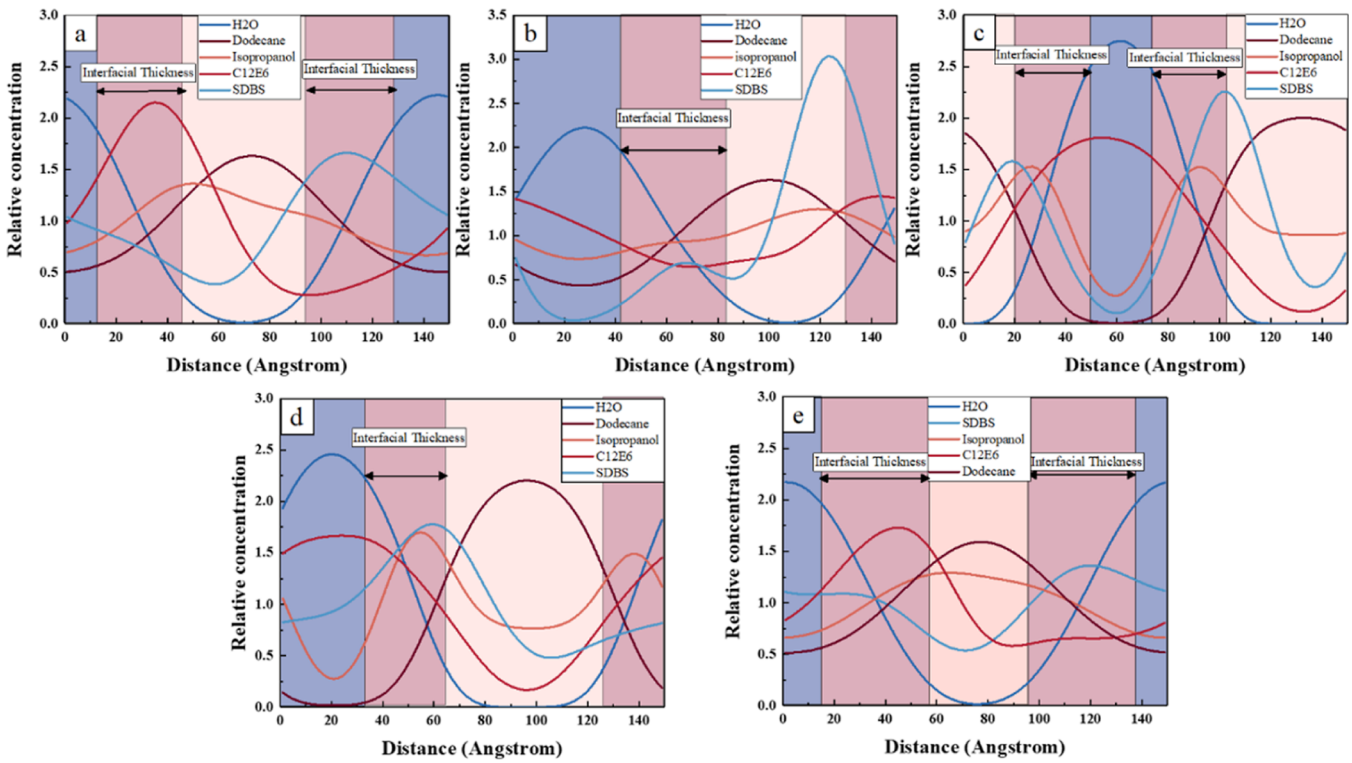

Figure 8. Relative concentration profiles of different component systems along the *X* axis direction. Surfactant mole fraction: (a) C12E6 0.1249 and SDBS 0.8751; (b) C12E6 0.2755 and SDBS 0.7245; (c) C12E6 0.4611 and SDBS 0.5389; (d) C12E6 0.6953 and SDBS 0.3047; (e) C12E6 0.8373 and SDBS 0.1627; and in the graph, the light red region is the aggregation area of dodecane, the blue region is the aggregation area of water, and the red region is the area of interfacial membrane.

the other hand, the cosurfactant was distributed within the microemulsion, influencing the morphology of the interfacial film. The images demonstrate that altering the ratio of nonionic surfactants to anionic surfactants led to changes in the interface's morphology, despite the overall surfactant concentration remaining constant. The distribution and movement of the components can be analyzed by using various analytical tools.

https://doi.org/10.1021/acsomega.4c01933
ACS Omega 2024, 9, 23903−23916

The performance of the microemulsion is directly influenced by the characteristics of the interfacial film. A loosely distributed interfacial film can result in a decreased stability of the microemulsion. In the molecular dynamic simulation, the region of the interfacial film was determined using the 90−10 criterion[58] along the *X*-axis. According to this criterion, the interfacial film is considered to start when the density of the water beads reaches 90% of its peak value. Similarly, it is considered to terminate when the density of the aqueous phase reaches 10% of its peak value. The extent of the interfacial film is shown in the red region of Figure 8.

The thicknesses of the interfacial films of the antagonistic systems (C12E6 molar concentrations of 0.2755 and 0.8373) were 38.1 and 42.06 Å, respectively, whereas those of the synergistic systems (C12E6 molar concentrations of 0.1249 and 0.6953) were 32.6 and 31.6 Å. The thicknesses of the interfacial films of the microemulsions generated by the antagonistic surfactant systems were significantly higher than those of the synergistic systems. The thickness of the interfacial film of the microemulsion produced by the antagonistic surfactant system was significantly higher than that of the synergistic microemulsion, while the system with the best synergistic effect (C12E6 molar concentration 0.4611) had the most concentrated interfacial film of the microemulsion (29.2 Å). Analysis of the different components reveals that in the antagonistic system (C12E6 molar concentration of 0.2755), SDBS does not have the highest molar ratio but produces the most aggregated peak of all of the systems, with a relative concentration value of 3.02. The excessively high relative concentration of SDBS suggests that in the interfacial membrane, SDBS repels mixing with C12E6, and in the interfacial membrane, the high relative concentration of SDBS indicates that SDBS rejects mixing with C12E6 at the interfacial membrane and occupies an area at the interfacial membrane alone to isolate itself from C12E6, which is also a manifestation of the antagonistic effect of this system at the microscopic level.

From the perspective of cosurfactant distribution, it was observed that the main peak of the cosurfactant did not appear at the position of surfactant aggregation in the antagonistic systems (C12E6 molar fractions of 0.8373 and 0.2755). This finding indicates that the surfactant could not effectively synergize with the additives under these ratios. Additionally, in the case of a C12E6 molar fraction of 0.1249, although a more concentrated interfacial film and stable oil−water distribution were achieved, the aggregation peak of SDBS at low concentration was the highest among all the ratios. This high peak suggests a poor synergistic effect. In the C12E6 molar fractions 0.1249 system, which also exhibits a synergistic effect, the cosurfactant fails to exhibit improved distribution behavior due to its low proportion in the system.

3.3.1. Surface Tension Analysis. IFT on a planar surface is calculated using the method of Irving−Kirkwood,[59] as depicted in eq 12. This calculation is based on the components of the pressure tensor of microemulsion droplets in three directions. It also considers the IFT between the oil and water phases, which is influenced by an interfacial film formed by the surfactant and cosurfactant. The last three frames (0.3 ns) after model stabilization were analyzed for each scaling regime and errors were accounted for. The oil−water IFT in each model was determined using an IFT calculation script.[60]

$$\gamma = L_Z\left[\langle P_{ZZ}\rangle - \frac{1}{2}(\langle P_{XX}\rangle + \langle P_{YY}\rangle)\right] \quad (12)$$

Where γ are IFT, mN/m; L_Z are the length of the model, Å; P_{ZZ}, P_{XX}, and P_{YY} are the pressure components of the microemulsion in the three directions.

In the model presented in this paper, the initial random distribution of all components results in the final formation of the oil−water interfacial film not being uniformly directed (such as P_{XX}). Therefore, when calculating IFT, the direction is selected based on the direction of the interfacial film of the emulsion. The IFT of the microemulsion model with different surfactant molar ratios is shown in Figure 9.

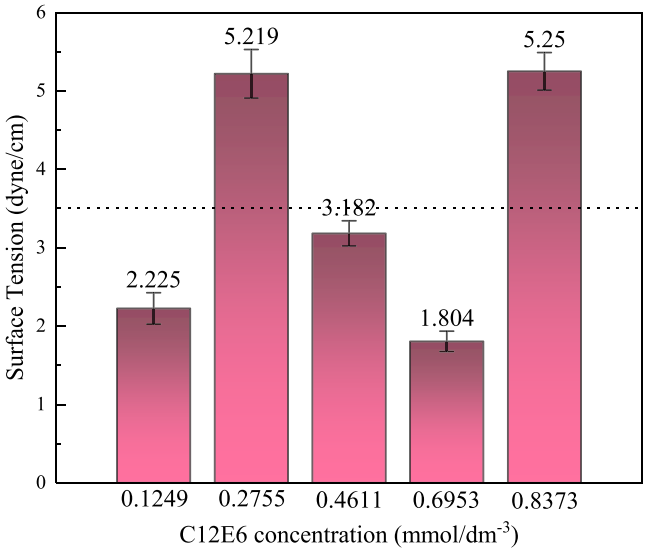

Figure 9. IFT between oil and water phases in microemulsions with varying molar ratios of C12E6 (the error bar data are derived from the last three frames of the model's IFT).

The change of IFT between oil and water can reflect the performance of the interfacial film formed by the surfactant and cosurfactant. From the IFT between the oil phase and the water phase, it can be found that the IFT between the oil phase and the water phase of the microemulsion formed by two groups of surfactant systems (C12E6 mole fractions of 0.2755 and 0.8373) with antagonistic effects screened by the Clint model is higher, while the IFT between the oil and water phases of the microemulsion formed by C12E6 mole fractions of 0.1249, 0.4611, and 0.6953 is lower. The results show that the synergy and antagonism between surfactants will affect the interaction between the oil phase and water phase during the formation of microemulsion. However, it can also be found that when the C12E6 mole fraction is 0.1249, 0.4611, and 0.6953, the IFT between the oil phase and water phase is not the lowest among all systems. The synergy and antagonism will affect the formation of microemulsion to some extent, but the performance of microemulsion is also composed of the stability of interface film and other aspects.

3.3.2. Analysis of Mean Square Displacement of Microemulsion Components. The slope of the mean square displacement (MSD) with time is proportional to the diffusion coefficient of the molecules.[61] The diffusion coefficients of the molecules in the simulated system can be calculated from the simulated trajectories by the Einstein[62] equation of eq 13

https://doi.org/10.1021/acsomega.4c01933
ACS Omega 2024, 9, 23903−23916

$$D = \frac{1}{2N_d} \lim_{t\to\infty} \frac{d}{dt} \langle |\overrightarrow{r(t)} - \overrightarrow{r(0)}|^2 \rangle \quad (13)$$

where D is the diffusion coefficients, Angstrom;[2] N_d is the dimension of the simulated system ($N_d = 3$) and $r(t)$ and $r(0)$ are the positions of the calculated molecules at moment t and the initial moment, respectively. The diffusion coefficients of the different components as a function of the molar ratio of C12E6 are shown in Figure 10.

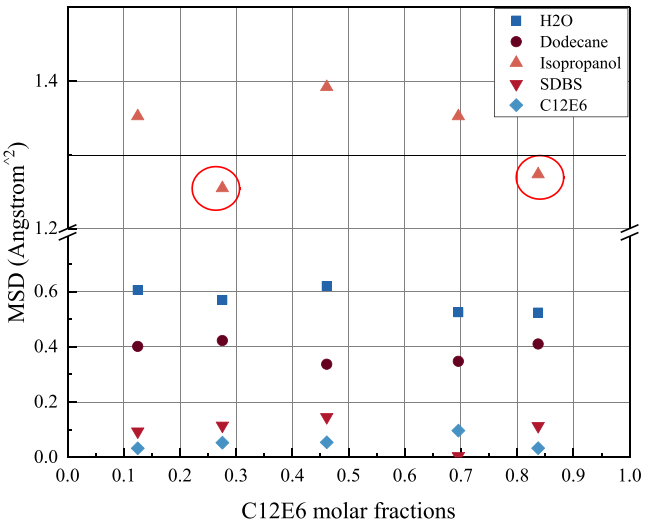

Figure 10. Plot of diffusion coefficients of different fractions as a function of the molar ratio of C12E6 (red circles indicate systems with smaller diffusion coefficients for isopropanol).

The diffusion coefficients of the two surfactants are small relative to other substances because of their large molecular weights and relatively fixed distribution positions (forming interfacial membranes); the diffusion coefficients of the water molecules are higher than those of the oil phase because of their smaller molecular weights and lower content relative to dodecane, which is in agreement with the law of water-in-oil microemulsions in other papers. The small molecule cosurfactant isopropanol (isopropanol) has the largest diffusion ability because it can be distributed in the oil phase, water phase, and interfacial film simultaneously, and the diffusion coefficient of isopropanol is smaller in the model that produces antagonistic effect, systems as marked by red circles, the synergism between surfactants affects the formation of the interfacial film,[63] and the poorer interfacial film properties will hinder the movement and final stabilization of the small molecule isopropanol, which will lead to the decrease of diffusion coefficient.

3.3.3. Radial Distribution Function Analysis. The radial distribution function (RDF) is the ratio of the regional density to the average density of the system, which can reflect the aggregation of components, and is calculated using eq 14

$$g(r) = \frac{1}{4\pi^2 \delta r} \cdot \frac{\sum_{t=1}^{T} \sum_{j=1}^{N} \Delta N(r \to r + \delta r)}{NT} \quad (14)$$

where ρ is the total density of the simulated system; r is the distance between two beads when calculating the RDF; N is the total number of molecules in the simulated system, and T is the total number of steps in the simulation calculation; δr is the difference in distances set to be calculated; and ΔN is the

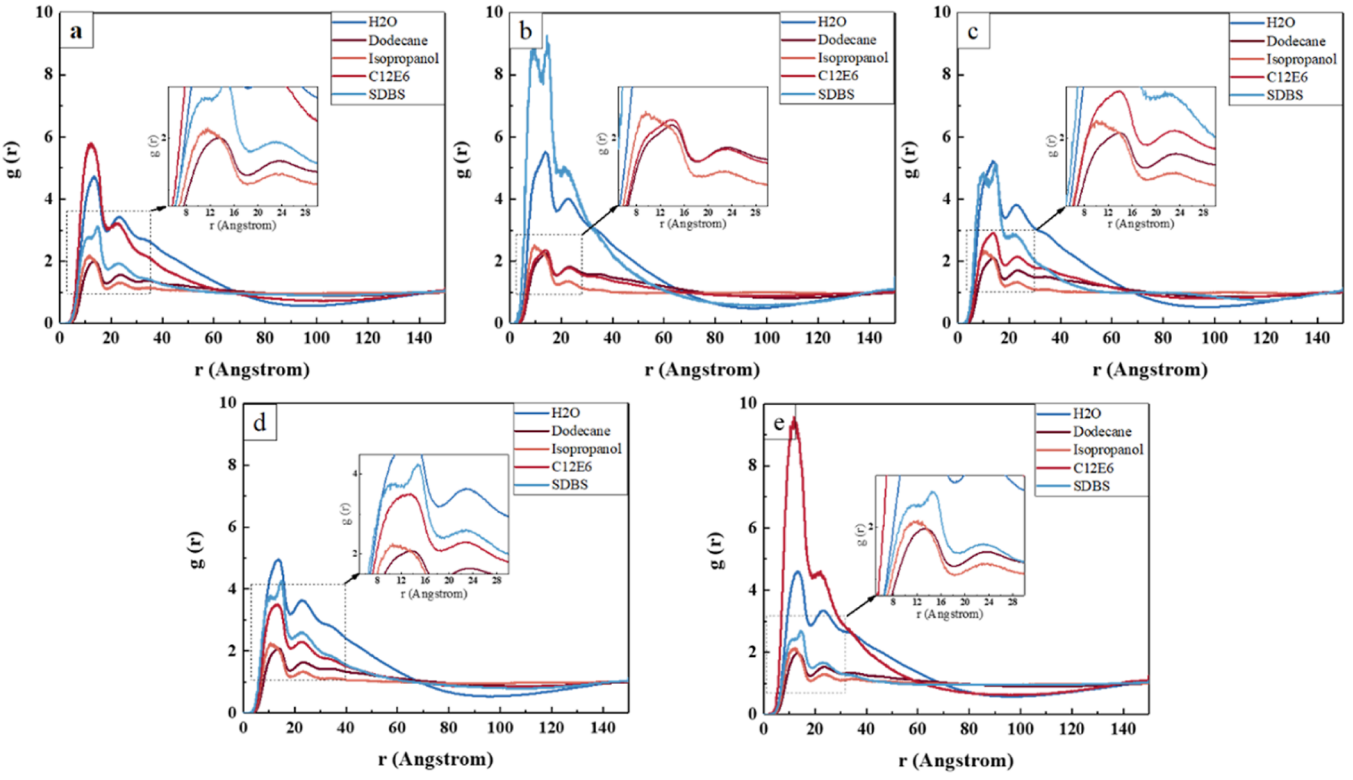

Figure 11. Radial distribution functions of microemulsions by different molar fraction ratios of the surfactant. Surfactant mole fraction: (a) C12E6 0.1249 and SDBS 0.8751; (b) C12E6 0.2755 and SDBS 0.7245; (c) C12E6 0.4611 and SDBS 0.5389; (d) C12E6 0.6953 and SDBS 0.3047; and (e) C12E6 0.8373 and SDBS 0.1627.

https://doi.org/10.1021/acsomega.4c01933
ACS Omega 2024, 9, 23903−23916

total number of coarsely grained beads with distances between $r \rightarrow r + \delta r$. The RDFs of microemulsions with different molar fraction ratios of surfactants are shown in Figure 11.

In the simulated system, as the distance approaches infinity, the value of $g(r)$ converges to 1, indicating that the overall density of the system is stable. Within this system, the cosurfactant exhibits a relatively small peak due to its broad distribution and a certain degree of aggregation on the interfacial film. The system generates water-in-oil microemulsions due to the oil−water ratio with the oil phase serving as the dispersed phase. Consequently, the degree of aggregation is lower in comparison to that of the water phase.

The aggregation behavior of surfactants in microemulsions is closely tied to the synergistic effect of the surfactants. In the microemulsion with a C12E6 molar fraction of 0.8373, the maximum aggregation peak of C12E6 at 12 Å is 9.2. However, in the microemulsion created with an C12E6 molar fraction of 0.2755, the maximum aggregation peak across all ratios is seen in SDBS. It is observed that at the C12E6 aggregation peak, the SDBS peak appears to decrease, indicating that SDBS aggregation avoids C12E6 concentration. Surfactant systems with poorer synergistic effects show much higher $g(r)$ values for a single surfactant than other systems after microemulsion formation. This phenomenon also demonstrates the antagonistic effect between the surfactants in this molar fraction system. In the microemulsion with a C12E6 molar fraction of 0.1249, despite the lower molar fraction of C12E6, its aggregation peaks are still higher than those of the two systems with better synergistic effect (C12E6 molar fractions of 0.4611 and 0.6953). The low proportion of C12E6 fails to produce good distribution behavior with anionic surfactant SDBS, although it can produce a synergistic effect to reduce the CMC. In contrast, for the two groups with better synergistic effect (C12E6 molar fractions 0.4611 and 0.6953), none of the surfactants produce excessive aggregation, thereby proving the synergistic effect of these surfactants molar fractions.

4. CONCLUSIONS

The Clint model of surfactant micellization and the experimentally measured CMC (CMC_{mix}) of the mixed solution indicate the synergistic effect between surfactants. When the molar fraction of C12E6 is 0.1249, 0.4611, or 0.6953, the CMC_{mix} is lower than the CMC_{id}, indicating a synergistic interaction between the nonionic and anionic surfactants. Conversely, when the molar fractions of C12E6 are 0.2755 or 0.8373, CMC_{mix} is higher than CM_{Cid}, suggesting an antagonistic interaction between the nonionic and anionic surfactants. The change in surfactant composition ratios leads to alterations in the synergistic effect between these surfactants. Analyzing the microemulsion particle size distribution revealed that systems with good synergistic effect produced smaller particle sizes and exhibited better stability when subjected to changes in inorganic salt concentration.

Modeling and analyzing microemulsions using the DPD model demonstrated that systems with excellent synergistic effect possess desirable properties at the microscopic level. Density distribution analysis showed that microemulsion systems with a synergistic effect exhibit more stable interfacial film morphology and distribution. Additionally, these systems effectively reduce the IFT between the oil and water phases of the microemulsion. Conversely, surfactant systems with an antagonistic effect, as identified by Clint's model, form microemulsions with higher interfacial tensions between the oil and water phases. Diffusion coefficient analysis revealed that cosurfactant diffusion coefficients are lower in antagonistic models. The synergism between surfactants affects the formation of interfacial films, and poorer interfacial film properties hinder the stabilization of the cosurfactant. Analysis of the RDF showed that active agent systems with a weaker synergistic effect exhibit higher values of $g(r)$ for each surfactant after microemulsion formation. The interactions between surfactants directly affect the microscopic properties of microemulsions.

In conclusion, changes in the molar fractions of anionic and nonionic surfactant systems induce variations in their synergistic and antagonistic effects, which subsequently affect the properties of the resulting microemulsions. In this paper, we have innovatively analyzed the properties and stability of microemulsions from a more microscopic point of view, starting from the Clint model of surfactant synergism and using a DPD model approach. These outcomes can be predicted and estimated by using the Clint model. The molecular dynamics and dissipative dynamics models provide effective analytical methods for evaluating the structure and properties of microemulsions at the microscopic level. Based on this methodology and theory, it is possible to efficiently screen microemulsions formed by different types of nonionic and anionic surfactants and to rapidly screen microemulsion formulations for microemulsions for enhanced recovery.

■ ASSOCIATED CONTENT

Supporting Information

The Supporting Information is available free of charge at https://pubs.acs.org/doi/10.1021/acsomega.4c01933.

Surface tension calculation and surface tension test size of the droplets and surface tension test method; composition and formulation of microemulsions generated by surfactant systems with different molar ratios; and repulsive force parameters between different beads in the DPD simulations (PDF)

■ AUTHOR INFORMATION

Corresponding Author

Baoshan Guan − *Research Institute of Percolation Fluids Mechanics, Chinese Academy of Sciences, Beijing 100010, China; Research Institute of Petroleum Exploration and Development, Beijing 100010, China;* orcid.org/0009-0004-6285-7074; Phone: +86-13008116613; Email: gbs7611@163.com

Authors

Biao Zhang − *Research Institute of Percolation Fluids Mechanics, Chinese Academy of Sciences, Beijing 100010, China*

Yufan Tao − *Research Institute of Percolation Fluids Mechanics, Chinese Academy of Sciences, Beijing 100010, China*

Weidong Liu − *Research Institute of Percolation Fluids Mechanics, Chinese Academy of Sciences, Beijing 100010, China; Research Institute of Petroleum Exploration and Development, Beijing 100010, China*

Baoliang Peng − *Research Institute of Petroleum Exploration and Development, Beijing 100010, China*

https://doi.org/10.1021/acsomega.4c01933
ACS Omega 2024, 9, 23903−23916

Kai Lv − *Research Institute of Percolation Fluids Mechanics, Chinese Academy of Sciences, Beijing 100010, China*

Complete contact information is available at: https://pubs.acs.org/10.1021/acsomega.4c01933

Author Contributions

Conceptualization, B.Z.; investigation, B.Z., Y.T., and K.L; review and editing, B.G. and W.L.; supervision, B.P. and S.C.; and funding acquisition, W.L. and B.P. All authors have read and agreed to the published version of the manuscript.

Notes

The authors declare no competing financial interest.

■ ACKNOWLEDGMENTS

This work was supported by the National Natural Science Foundation of China (22008263).

■ REFERENCES

(1) (a) Alvarado, V.; Manrique, E. Enhanced Oil Recovery: An Update Review. *Energies* **2010**, *3* (9), 1529−1575. (b) Mai, A.; Kantzas, A. Mechanisms of Heavy Oil Recovery by Low Rate Waterflooding. *J. Can. Pet. Technol.* **2010**, *49* (03), 44−50.

(2) (a) Muggeridge, A.; Cockin, A.; Webb, K.; Frampton, H.; Collins, I.; Moulds, T.; Salino, P. Recovery rates, enhanced oil recovery and technological limits. *Philos. Trans. R. Soc., A* **2014**, *372* (2006), 20120320. (b) Patel, J.; Borgohain, S.; Kumar, M.; Rangarajan, V.; Somasundaran, P.; Sen, R. Recent developments in microbial enhanced oil recovery. *Renewable Sustainable Energy Rev.* **2015**, *52*, 1539−1558.

(3) Chen, W. D.; Geng, X. F.; Liu, W. D.; Ding, B.; Xiong, C. M.; Sun, J. F.; Wang, C.; Jiang, K. A Comprehensive Review on Screening, Application, and Perspectives of Surfactant-Based Chemical-Enhanced Oil Recovery Methods in Unconventional Oil Reservoirs. *Energy Fuels* **2023**, *37* (7), 4729−4750.

(4) (a) SunLiang, S. S.; Liu, Y.; Liu, D.; Gao, M.; Tian, Y.; Wang, J.; Wang, J. K. A review on shale oil and gas characteristics and molecular dynamics simulation for the fluid behavior in shale pore. *J. Mol. Liq.* **2023**, *376*, 121507. (b) Jing, W.; Huiqing, L.; Genbao, Q.; Yongcan, P.; Yang, G. Investigations on spontaneous imbibition and the influencing factors in tight oil reservoirs. *Fuel* **2019**, *236*, 755−768.

(5) (a) WeverPicchioni, D. F.; Broekhuis, A.; Broekhuis, A. A. Polymers for enhanced oil recovery: A paradigm for structure-property relationship in aqueous solution. *Prog. Polym. Sci.* **2011**, *36* (11), 1558−1628. (b) Isaac, O. T.; Pu, H.; Oni, B. A.; Samson, F. A. Surfactants employed in conventional and unconventional reservoirs for enhanced oil recovery—A review. *Energy Rep.* **2022**, *8*, 2806−2830.

(6) (a) GbadamosiPatil, A. S.; Al Shehri, D.; Kamal, M. S.; Hussain, S. S.; Al-Shalabi, E. W.; Hassan, A. M.; Hassan, A. M. Recent advances on the application of low salinity waterflooding and chemical enhanced oil recovery. *Energy Rep.* **2022**, *8*, 9969−9996. (b) Raffa, P.; Broekhuis, A. A.; Picchioni, F. Polymeric surfactants for enhanced oil recovery: A review. *J. Pet. Sci. Eng.* **2016**, *145*, 723−733.

(7) Olajire, A. A. Review of ASP EOR (alkaline surfactant polymer enhanced oil recovery) technology in the petroleum industry: Prospects and challenges. *Energy* **2014**, *77*, 963−982.

(8) Zhu, Y. Y.; Hou, Q. F.; Jian, G. Q.; Ma, D. S.; Wang, Z. Current development and application of chemical combination flooding technique. *Pet. Explor. Dev.* **2013**, *40* (1), 96−103.

(9) Hon, V. Y.; Saaid, I. M.; Chai, I. C. H.; Fauzi, N. A. A. M.; Deguillard, E.; van Male, J.; Handgraaf, J.-W. Microemulsion interface model for chemical enhanced oil recovery design. *J. Pet. Sci. Eng.* **2022**, *212*, 110279.

(10) (a) Mariyate, J.; Bera, A. Recent progresses of microemulsions-based nanofluids as a potential tool for enhanced oil recovery. *Fuel* **2021**, *306*, 121640. (b) Romero-Zern, L. *Introduction to Enhanced Oil Recovery (EOR) Processes and Bioremediation of Oil-Contaminated Sites*; IntechOpen, 2012.

(11) (a) PaulMoulik, B. K. S. P.; Moulik, S. P. Microemulsions: An overview. *J. Dispersion Sci. Technol.* **1997**, *18* (4), 301−367. (b) Mason, T. G.; Wilking, J. N.; Meleson, K.; Chang, C. B.; Graves, S. M. Nanoemulsions: formation, structure, and physical properties. *J. Phys.-Condes. Matter* **2006**, *18* (41), R635−R666.

(12) (a) Torchilin, V. P. Micellar nanocarriers: pharmaceutical perspectives. *Pharm. Res.* **2006**, *24* (1), 1−16. (b) Lawrence, M. J.; Rees, G. D. Microemulsion-based media as novel drug delivery systems. *Adv. Drug Delivery Rev.* **2000**, *45* (1), 89−121.

(13) Zhu, T.; Kang, W.; Yang, H.; Li, Z.; Zhou, B.; He, Y.; Wang, J.; Aidarova, S.; Sarsenbekuly, B. Advances of microemulsion and its applications for improved oil recovery. *Adv. Colloid Interface Sci.* **2022**, *299*, 102527.

(14) Pal, N.; Kumar, S.; Bera, A.; Mandal, A. Phase behaviour and characterization of microemulsion stabilized by a novel synthesized surfactant: Implications for enhanced oil recovery. *Fuel* **2019**, *235*, 995−1009.

(15) Bera, A.; Mandal, A. Microemulsions: a novel approach to enhanced oil recovery: a review. *J. Pet. Explor. Prod. Technol.* **2015**, *5* (3), 255−268.

(16) Mariyate, J.; Bera, A. A critical review on selection of microemulsions or nanoemulsions for enhanced oil recovery. *J. Mol. Liq.* **2022**, *353*, 118791.

(17) Strey, R. Microemulsion microstructure and interfacial curvature. *Colloid Polym. ScI.* **1994**, *272* (8), 1005−1019.

(18) Hirasaki, G. J.; Miller, C. A.; Puerto, M. Recent Advances in Surfactant EOR. *SPE J.* **2011**, *16* (04), 889−907.

(19) (a) Broens, M.; Unsal, E. Emulsification kinetics during quasi-miscible flow in dead-end pores. *Adv. Water Resour.* **2018**, *113*, 13−22. (b) Abdelfatah, E.; Wahid-Pedro, F.; Melnic, A.; Vandenberg, C.; Luscombe, A.; Berton, P.; Bryant, S. L. Microemulsion Formulations with Tunable Displacement Mechanisms for Heavy Oil Reservoirs. *SPE J.* **2020**, *25* (05), 2663−2677.

(20) (a) FlaatenNguyen, A. K. Q. P.; Pope, G. A.; Zhang, J.; Zhang, J. Y. A Systematic Laboratory Approach to Low-Cost, High-Performance Chemical Flooding. *SPE Reservoir Eval. Eng.* **2009**, *12* (05), 713−723. (b) Winsor, P. A. Hydrotropy, solubilisation and related emulsification processes. *Trans. Faraday Soc.* **1948**, *44* (7), 451−455.

(21) Healy, R. N.; Reed, R. L.; Stenmark, D. G. Multiphase Microemulsion Systems. *SPE J.* **1976**, *16* (03), 147−160.

(22) Gradzielski, M.; Duvail, M.; de Molina, P. M.; Simon, M.; Talmon, Y.; Zemb, T. Using Microemulsions: Formulation Based on Knowledge of Their Mesostructure. *Chem. Rev.* **2021**, *121* (10), 5671−5740.

(23) Kahlweit, M.; Strey, R.; Haase, D.; Kunieda, H.; Schmeling, T.; Faulhaber, B.; Borkovec, M.; Eicke, H. F.; Busse, G.; Eggers, F.; et al. How to study microemulsions. *J. Colloid Interface Sci.* **1987**, *118* (2), 436−453.

(24) Bansal, V. K.; Shah, D. O. Microemulsions and Tertiary Oil Recovery. *Microemulsions Theory and Practice*; Academic Press, 1977.

(25) Prince, L. M. *Microemulsions Theory and Practice*; Elsevier, 1977.

(26) Scriven, L. Equilibrium bicontinuous structure. *Nature* **1976**, *263* (5573), 123−125.

(27) (a) Prince, M. L. *Microemulsions Theory and Practice*; Erdol Kohle Erdgas Petrochem., 1977. (b) Paunov, V. N.; Sandler, S. I.; Kaler, E. W. A simple molecular model for the spontaneous curvature and the bending constants of nonionic surfactant monolayers at the oil/water interface. *Langmuir* **2000**, *16* (23), 8917−8925.

(28) Schneider, K.; Ott, T. M.; Schweins, R.; Frielinghaus, H.; Lade, O.; Sottmann, T. Phase Behavior and Microstructure of Symmetric Nonionic Microemulsions with Long-Chain n-Alkanes and Waxes. *Ind. Eng. Chem. Res.* **2019**, *58* (7), 2583−2595.

(29) Herrera, D.; Chevalier, T.; Frot, D.; Barre, L.; Drelich, A.; Pezron, I.; Dalmazzone, C. Monitoring the formation kinetics of a

bicontinuous microemulsion. *J. Colloid Interface Sci.* **2022**, *609*, 200−211.
(30) Zhao, X.; Zhan, F.; Liao, G.; Liu, W.; Su, X.; Feng, Y. In situ micro-emulsification during surfactant enhanced oil recovery: A microfluidic study. *J. Colloid Interface Sci.* **2022**, *620*, 465−477.
(31) Carrillo, C. A.; Saloni, D.; Lucia, L. A.; Hubbe, M. A.; Rojas, O. J. Capillary flooding of wood with microemulsions from Winsor I systems. *J. Colloid Interface Sci.* **2012**, *381* (1), 171−179.
(32) (a) PošaPoša, M. M. Mixed micelles of binary surfactant mixtures Tween 40 − Na-3,12-dioxo-5β-cholanate and Tween 80 − Na-3,12-dioxo-5β-cholanate and their thermodynamic description and characterization. *Chem. Eng. Res. Des.* **2014**, *92* (12), 2826−2839. (b) Holland, P. M.; Rubingh, D. N. Nonideal Multicomponent Mixed Micelle Model. *J. Phys. Chem.* **1983**, *87* (11), 1984−1990.
(33) Sripriya, R.; Muthu Raja, K.; Santhosh, G.; Chandrasekaran, M.; Noel, M. The effect of structure of oil phase, surfactant and co-surfactant on the physicochemical and electrochemical properties of bicontinuous microemulsion. *J. Colloid Interface Sci.* **2007**, *314* (2), 712−717.
(34) (a) RenLiu, S. X.; Lin, P.; Gao, Y.; Erkens, S.; Erkens, S. Molecular dynamics simulation on bulk bitumen systems and its potential connections to macroscale performance: Review and discussion. *Fuel* **2022**, *328*, 125382. (b) Mehana, M.; Kang, Q. J.; Nasrabadi, H.; Viswanathan, H. Molecular Modeling of Subsurface Phenomena Related to Petroleum Engineering. *Energy Fuels* **2021**, *35* (4), 2851−2869. (c) Li, Y.-M.; Yuan, S.-L.; Xu, G.-Y. Applications of Computer Simulation in the Study of Surfactant System. *Acta Phys. -Chim. Sin.* **2003**, *19*, 986.
(35) Fu, L.; Gu, F.; Liao, K.; Wen, X.; Huang, W.; Li, X.; Ren, Z.; Xie, L. Application of molecular simulation in tertiary oil recovery: A systematic review. *J. Pet. Sci. Eng.* **2022**, *212*, 110196.
(36) Tandon, K.; Fraaije, J. G. E. M.; Jain, A.; Handgraaf, J. W.; Buijse, M. A.; Jain, S. Accelerated Surfactant Selection for EOR Using Computational Methods. *SPE Enhanced Oil Recovery Conference*, 2013.
(37) Santo, K. P.; Neimark, A. V. Dissipative particle dynamics simulations in colloid and Interface science: a review. *Adv. Colloid Interface Sci.* **2021**, *298*, 102545.
(38) Liu, M. B.; Liu, G. R.; Zhou, L. W.; Chang, J. Z. Dissipative Particle Dynamics (DPD): An Overview and Recent Developments. *Arch. Comput. Methods Eng.* **2015**, *22* (4), 529−556.
(39) Hoogerbrugge, P. J.; Koelman, J. Simulating Microscopic Hydrodynamic Phenomena with Dissipative Particle Dynamics. *Europhys. Lett.* **1992**, *19* (3), 155−160.
(40) (a) LiTang, Z. Y. H.; Li, X.; Karniadakis, G. E.; Karniadakis, G. E. Mesoscale modeling of phase transition dynamics of thermoresponsive polymers. *Chem. Commun.* **2015**, *51* (55), 11038−11040. (b) Litvinov, S.; Hu, X.; Ellero, M.; Adams, N. Mesoscopic simulation of the transient behavior of semi-diluted polymer solution in a microchannel following extensional flow. *Microfluid. Nanofluid.* **2014**, *16* (1−2), 257−264.
(41) (a) AlasiriSultan, H. S. A. S.; Chapman, W. G.; Chapman, W. G. Effect of Surfactant Headgroup, Salts, and Temperature on Interfacial Properties: Dissipative Particle Dynamics and Experiment for the Water/Octane/Surfactant System. *Energy Fuels* **2019**, *33* (7), 6678−6688. (b) Choudhary, M.; Kamil, S. M. Phase Diagram Study of Catanionic Surfactants Using Dissipative Particle Dynamics. *ACS Omega* **2022**, *7* (33), 29306−29325.
(42) Al-Lehyani, I. H.; Grime, J. M. A.; Bano, M.; McKelvey, K.; Allen, M. P. Coarse-grained simulation of transmembrane peptides in the gel phase. *J. Comput. Phys.* **2013**, *238*, 97−105.
(43) Li, Y.; Zhang, P.; Dong, F.-L.; Cao, X.-L.; Song, X.-W.; Cui, X.-H. The array and interfacial activity of sodium dodecyl benzene sulfonate and sodium oleate at the oil/water interface. *J. Colloid Interface Sci.* **2005**, *290* (1), 275−280.
(44) Bagheri, A.; Ahmadi, S. M. A. Mixed micellization between amphiphilic drug propranolol hydrochloride and cetyltrimethylammonium bromide surfactant in aqueous medium. *J. Mol. Liq.* **2017**, *230*, 254−260.
(45) Harkins, W. D.; Jordan, H. F. A method for the determination of surface and interfacial tension from the maximum pull on a ring. *J. Am. Chem. Soc.* **1930**, *52*, 1751.
(46) Barari, M.; Ramezani, M.; Lashkarbolooki, M.; Abedini, R. Influence of alkyl chain length of imidazolium-based ionic liquid on the crude oil-aqueous solution IFT under different ionic strengths. *Fluid Phase Equilib.* **2022**, *556*, 113404.
(47) Groot, R. D.; Madden, T. J. Dynamic simulation of diblock copolymer microphase separation. *J. Chem. Phys.* **1998**, *108* (20), 8713−8724.
(48) Lee, M. T.; Mao, R. F.; Vishnyakov, A.; Neimark, A. V. Parametrization of Chain Molecules in Dissipative Particle Dynamics. *J. Phys. Chem. B* **2016**, *120* (22), 4980−4991.
(49) Guan, D.; Feng, S.; Zhang, L.; Shi, Q.; Zhao, S.; Xu, C. Mesoscale Simulation for Heavy Petroleum System Using Structural Unit and Dissipative Particle Dynamics (SU-DPD) Frameworks. *Energy Fuels* **2019**, *33* (2), 1049−1060.
(50) Ruiz-Morales, Y.; Mullins, O. C. Coarse-Grained Molecular Simulations to Investigate Asphaltenes at the Oil-Water Interface. *Energy Fuels* **2015**, *29*, 1597−1609.
(51) Zhang, D. N.; Shangguan, Q. Q.; Wang, Y. X. An easy-to-use boundary condition in dissipative particle dynamics system. *Comput. Fluids* **2018**, *166*, 117−122.
(52) Jiang, L.; Li, S.; Yu, W.; Wang, J.; Sun, Q.; Li, Z. Interfacial study on the interaction between hydrophobic nanoparticles and ionic surfactants. *Colloids Surf., A* **2016**, *488*, 20−27.
(53) Song, F.; Zhou, J. J.; Jia, Z. D.; He, L.; Sui, H.; Li, X. A. Interfacial behaviors of ionic liquids in petroleum Production: A review. *J. Mol. Liq.* **2023**, *382*, 121864.
(54) Motomura, K.; Yamanaka, M.; Aratono, M. Thermodynamic Consideration Of The Mixed Micelle Of Surfactants. *Colloid Polym. Sci.* **1984**, *262* (12), 948−955.
(55) Clint, J. H. Micellization of mixed nonionic surface-active agents. *J. Chem. Soc., Faraday Trans. 1* **1975**, *71*, 1327−1334.
(56) Hao, L. S.; Deng, Y. T.; Zhou, L. S.; Ye, H.; Nan, Y. Q.; Hu, P. Mixed Micellization and the Dissociated Margules Model for Cationic/Anionic Surfactant Systems. *J. Phys. Chem. B* **2012**, *116* (17), 5213−5225.
(57) Mariyate, J.; Bera, A. A critical review on selection of microemulsions or nanoemulsions for enhanced oil recovery. *J. Mol. Liq.* **2022**, *353*, 118791.
(58) (a) Gurbulak, O.; Cebe, E. Molecular dynamics study of 5CB at the air-water interface: From gas to beyond the monolayer collapse. *J. Mol. Liq.* **2018**, *256*, 611−619. (b) Rivera, J. L.; McCabe, C.; Cummings, P. T.; Cummings, P. T. Molecular simulations of liquid-liquid interfacial properties: Water-n-alkane and water-methanol-n-alkane systems. *Phys. Rev. E* **2003**, *67* (1), 011603. (c) Parra, J. G.; Iza, P.; Dominguez, H.; Schott, E.; Zarate, X. Effect of Triton X-100 surfactant on the interfacial activity of ionic surfactants SDS, CTAB and SDBS at the air/water interface: A study using molecular dynamic simulations. *Colloids Surf., A* **2020**, *603*, 125284.
(59) Lee, S. H. Pressure Analyses at the Planar Surface of Liquid-Vapor Argon by a Test-Area Molecular Dynamics Simulation. *Bull. Korean Chem. Soc.* **2012**, *33* (9), 3039−3042.
(60) Li, Y.; Guo, Y.; Xu, G.; Wang, Z.; Bao, M.; Sun, N. Dissipative particle dynamics simulation on the properties of the oil/water/surfactant system in the absence and presence of polymer. *Mol. Simul.* **2013**, *39* (4), 299−308.
(61) Li, J.; Han, Y.; Qu, G. M.; Cheng, J. C.; Xue, C. L.; Gao, X.; Sun, T.; Ding, W. Molecular dynamics simulation of the aggregation behavior of N-Dodecyl-N, N-Dimethyl-3-Ammonio-1-Propanesulfonate/sodium dodecyl benzene sulfonate surfactant mixed system at oil/water interface. *Colloids Surf., A* **2017**, *531*, 73−80.
(62) Zwanzig, R. W.; Kirkwood, J. G.; Stripp, K. F.; Oppenheim, I. The Statistical Mechanical Theory of Transport Processes. VI. A Calculation of the Coefficients of Shear and Bulk Viscosity of Liquids. *J. Chem. Phys.* **1953**, *21* (11), 2050−2055.

https://doi.org/10.1021/acsomega.4c01933
ACS Omega 2024, 9, 23903−23916

(63) Chilukoti, H. K.; Kikugawa, G.; Ohara, T. Self-diffusion Coefficient and Structure of Binary n-Alkane Mixtures at the Liquid-Vapor Interfaces. *J. Phys. Chem. B* **2015**, *119*, 13177−13184.

https://doi.org/10.1021/acsomega.4c01933
ACS Omega 2024, 9, 23903−23916